A EUROPEAN JOURNAL

CHEMPHYSCHEM

OF CHEMICAL PHYSICS AND PHYSICAL CHEMISTRY

Accepted Article

Title: Characterization of protonated model disaccharides from tandem mass spectrometry and chemical dynamics simulations

Authors: Estefania Rossich-Molina, Ane Eizaguirre, Violette Haldys, Dominique Urban, Gilles Doisneau, Yann Bourdreux, Jean-Marie Beau, Jean-Yves Salpin, and Riccardo Spezia

To be cited as: *ChemPhysChem* 10.1002/cphc.201700202

Link to VoR: http://dx.doi.org/10.1002/cphc.201700202

A Journal of

ChemPubSoc Europe

WILEY-VCH

www.chemphyschem.org

10.1002/cphc.201700202

WILEY-VCH

ARTICLE

Characterization of protonated model disaccharides from tandem mass spectrometry and chemical dynamics simulations

Estefania Rossich Molina,[a,b] Ane Eizaguirre,[a,b] Violette Haldys,[a,b] Dominique Urban,[c] Gilles Doisneau,[c] Yann Bourdreux,[c] Jean-Marie Beau,[c] Jean-Yves Salpin*[a,b] and Riccardo Spezia*[a,b]

Abstract: In the present work the fragmentation mechanisms of prototypical disaccharides have been studied by coupling tandem mass spectrometry (MS) with collisional chemical dynamics simulations. These last calculations were performed by explicitly considering the collisions between the protonated sugar and the neutral target gas, leading to an ensemble of trajectories for each system, from which it was possible to obtain reaction products and mechanisms without pre-imposing them. The β-aminoethyl and aminopropyl derivatives of cellobiose, maltose and gentiobiose were studied in order to see the differences in both the stereochemistry and the location of the glycosidic linkage. Chemical dynamics simulations of MS/MS and MS/MS/MS are used to suggest some primary and secondary fragmentation mechanisms for some experimentally observed product ions. The simulations performed provide some new insights about the fundamentals of unimolecular dissociation of protonated sugars under CID conditions.

Introduction

Carbohydrates, as part of glycoproteins and glycolipids involved in cell signaling, play an important biological role.[1] Besides their biological relevance, the characterization of both the structure and reactivity of carbohydrates is *per se* a challenging topic for spectrometric identification due to the numerous questions that have to be addressed, including the nature and position of the functional groups, the sites and anomeric configuration of the glycosidic linkages, and the stereochemical characterization of the different asymmetric centers of the sugar rings.

To study the intrinsic reactivity of carbohydrates by getting rid of their environment, gas-phase studies are pointed out as a satisfactory approach. In this respect, fast atom bombardment (FAB),[2] matrix assisted laser desorption ionization (MALDI),[3] desorption electrospray ionization (DESI)[4] or electrospray ionization (ESI)[5] techniques are particularly useful, and have been extensively used to generate bio-molecular ions in the gas phase. In combination with these ionization methods, tandem mass spectrometry (MS/MS) through collisional induced dissociation of ions (CID) are also particularly helpful to understand the unimolecular reactivity and to identify characteristic features of biomolecules, since activated ions get enough energy to follow extensive fragmentation.[6]

One difficult task of mass spectrometry in sugar chemistry is to achieve isomeric distinction. However, the possibility of applying CID to differentiate isomeric sugars is appealing due to the relative rapidity of such an analytical approach with respect to more time-consuming spectroscopic methods. Another possibility of improving separation of isobaric isomers is given by ion mobility as notably recently reported by Pagel and co-workers.[7]

In general, the fragmentation mechanisms of saccharides are less investigated from a fundamental point of view than other polymeric molecules, as, in particular, peptides.[8] Studies on fragmentation mechanisms are reported on simple saccharides (like lactose) pointing out the possibility of primary vs consecutive fragmentations also using H/D exchange and ^{18}O or ^{13}C labeling and quantum chemical calculations.[9] Earlier theoretical studies were reported estimating barriers and mechanisms for other systems.[10]

To investigate their reactivity under CID conditions we combined MS/MS experiments with chemical dynamics simulations of collision. The use of chemical dynamics to model CID phenomenon was pioneered by Hase and co-workers in studying CID of different systems,[11] and more recently in our group it was applied to elucidate reaction mechanisms of a series of organic and biological molecules, from urea to peptides, from uracil to doubly charged complexes formed by an ion and an organic molecule.[12] Concerning sugars, the first, and up to now unique, system investigated with this approach was galactose 6-sulfate, in which simulations were able to reproduce the most important experimental fragmentation pathways and identify the underlying mechanisms.[13] In fact, direct dynamics are able to provide information on the structure of the fragment ions obtained after collision of a gaseous precursor ion with an inert gas, and thus on the reaction pathways, without pre-imposing any reaction coordinate.

The next step of our work on sugars is to check if chemical dynamics simulations could also provide new insights on the mechanisms associated with the glycosidic bond cleavages, and if simulations could achieve isomeric distinction. To this end, we decided to study the simplest carbohydrates exhibiting an interglycosidic linkage, namely disaccharides. We have chosen three isomers, D-maltose, D-cellobiose and D-gentiobiose, which

[a] Dr. E. Rossich Molina, Dr. A. Eizaguirre, Mrs. V. Haldys, Dr. J.-Y. Salpin, Dr. R. Spezia
LAMBE, Univ Evry, CEA, CNRS, Université Paris-Saclay, F-91025 Evry, France
[b] Dr. E. Rossich Molina, Dr. A. Eizaguirre, Mrs. V. Haldys, Dr. J.-Y. Salpin, Dr. R. Spezia
LAMBE, Université Cergy-Pontoise, Université Paris-Seine, F-91025 Evry, France
E-mail: jeanyves.salpin@univ-evry.fr ; riccardo.spezia@univ-evry.fr
[c] Dr. D. Urban, Dr. G. Doisneau, Dr. Y. Bourdreux, Prof. J.-M. Beau
ICMMO – SM2B, Univ Paris-Sud, Université Paris-Saclay and CNRS F-91405 Orsay (France)

Supporting information for this article is given via a link at the end of the document.

differ from each other either by the position or the α,β-configuration of the glycosidic linkage. It has been shown that disaccharides could be easily distinguished by tandem mass spectrometry by performing MS/MS experiments on the $[M-H]^-$ pseudo-molecular ions.[14] However, several theoretical studies have demonstrated that the different hydroxyl groups of saccharides are of close acidity in the gas phase.[15] In addition, a recent report showed that C-deprotronation can also compete with O-deprotonation.[16] Consequently, the number of deprotonated forms to be considered in the negative mode being too high to perform chemical dynamics simulations, we decided to work in the positive-ion mode. However, in this case chemical derivatization was mandatory for two reasons. First, there is no preferred basic site since protonation of any of the O atoms of the sugars results in similar proton affinities.[17] Second, under electrospray conditions, $[M+H]^+$ ions of underivatized disaccharides are very weak as they easily fragment according to sequential losses of water molecules. Consequently, the three disaccharides were functionalized at the reducing end with amino-ethyl and amino-propyl groups (scheme 1), in order to unambiguously localize the positive charge for chemical dynamic simulations, and to generate intense $[M+H]^+$ ions that can then be easily studied by CID.

We have used the combination of experiments and chemical dynamics simulations to propose fragmentation mechanisms of these model disaccharide isomers and to investigate the possibility of differentiating them by CID experiments.

Methods

Organic synthesis. Aminoderivatives of cellobiose, maltose and gentiobiose were prepared following the same synthetic approach, which relies on β-selective glycosylations using a bromoalcohol, followed by appropriate functional group transformations. For all the required glycosides, the aglycone parts were β-selectively introduced using the common boron trifluoride-mediated glycosylation conditions,[18] with either 2-bromoethanol or 3-bromopropanol as the acceptor partner. Azido displacement of the bromine atom[19] followed by total deacetylation and reduction of the azido moiety delivered the β-aminoethyl and the β-aminopropyl glycosides.[19,20] The experimental conditions used are exemplified using the following preparation of the cellobiose derivatives in Scheme 2. Commercially available cellobiose was peracetylated using acetic anhydride in pyridine at room temperature overnight. The product was thus obtained with a yield of 95% as a 5:1 (α:β) mixture of isomers. The glycosylation was then carried out using 6 equivalents of 2-bromoethanol or 3-bromopropanol in dichloromethane and 6 equivalents of boron trifluoride etherate at room temperature for one hour. Flash chromatography purification gave the β-glycosides in 27% (n = 1) and 54% (n = 2). Next, treatment of the bromide derivatives with two equivalents of sodium azide in DMF at room temperature overnight, quantitatively yielded the azido products that were not purified. Total deacetylation under Zemplén conditions delivered the *O*-unprotected glycosides in 99% (n = 1) and 94% (n = 2) yields. Finally, the azido groups were converted into amino functionalities by palladium catalyzed hydrogenation reactions in methanol for two hours at room temperature. After filtration and evaporation of the solvent, the β-aminoethyl (n = 1) and the β-aminopropyl (n = 2) derivatives were obtained in yields of 70% and 90%, respectively. All glycosides were fully characterized and then lyophilized prior to their study by mass spectrometry. The synthesized disaccharides are schematically drawn in Scheme 1.

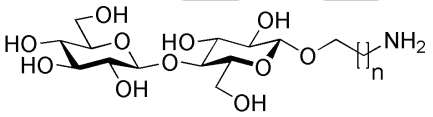

Cellobiosides (n = 1 and 2)

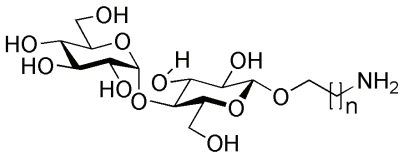

Maltobiosides (n = 1 and 2)

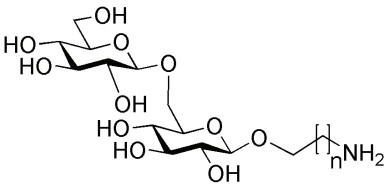

Gentiobiosides (n = 1)

Scheme 1. Aminoderivatives of Cellobiose (cellobiosides), Maltose (maltobiosides) and Gentiobiose (gentiobiosides) studied in the present work.

Scheme 2. Synthetic approach followed to prepare aminoderivatives of cellobiose, maltose and gentiobiose. For simplicity we show the cellobiose case.

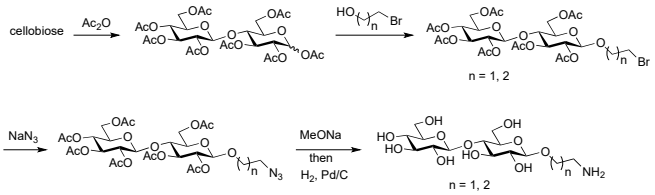

The preparation of the other aminoderivatives is similar.

Mass spectrometry experiments. Experiments were performed using an Applied Biosystems/MDS Sciex API2000 triple-quadrupole instrument fitted with a turboionspray source. Aqueous solutions (10^{-2} M) of β-aminoethyl and β-aminopropyl derivatives of Cellobiose β(1,4), Maltose α(1,4), Gentiobiose β(1,6) (synthetized as reported above) were diluted in Milli-Q water and were introduced in the source using direct infusion with a syringe pump at a flow rate of 5 µl/min. Ionization of the sample was achieved by applying a voltage of 5.5 kV on the sprayer probe and by the use of a nebulizing gas (GAS1, air) surrounding the sprayer probe, intersected by a heated gas (GAS2, air) at an

angle of 90°. The operating pressure of GAS1 and GAS2 are adjusted to 2.1 bars, by means of an electronic board (pressure sensors), as a fraction of the air inlet pressure. The curtain gas (N_2), which prevents air or solvent from entering the analyzer region, was similarly adjusted to a value of 1.4 bar. The temperature of GAS2 was set to 100°C. CID spectra were recorded by introducing nitrogen as collision gas in the second quadrupole.

Low gas pressures were used to limit multiple ion–molecule collisions. Moreover, the declustering potential (DP), defined as the difference of potentials between the "orifice plate" and the skimmer (grounded) was set to 40 V to perform MS/MS experiments. CID spectra were recorded at different collision energies ranging from 5 to 30 eV (laboratory frame). Note that MS/MS spectra are very likely obtained under a multiple-collision regime, and this increases the internal energy content of the precursor ion. With the CAD parameter (which controls the amount of N_2 introduced into Q2) set to its minimum value, the pressure value measured by the ion gauge, located at the vicinity of Q2, is about 3 × 10^{-5} Torr, but the actual pressure inside Q2 cannot be determined accurately. However, according to a report of the manufacturer,[21] this pressure inside Q2 is closer to 10^{-2} Torr. Given the dimensions of Q2, the mean free path for a moving N_2 molecule, according to the gas kinetic theory, is several mm at 10^{-2} Torr. Therefore a molecule of N_2 may undergo tens of collisions within Q2. This is a lower limit for the present ions, which have a larger diameter and, thus, a larger collision cross section.

We also recorded the CID spectrum of several fragment ions observed on the MS/MS spectra. To perform these MS/MS/MS "like" experiments, we operated as follows: from the obtained MS/MS spectrum, we first chose the fragment ions we wanted to dissociate. Then, we generated these fragment ions in the interface region of the instrument, by increasing the DP value to 60 V. Each fragment ion was then mass selected by Q1, transferred into Q2, where it collided with N_2 in the same way that it did for the MS/MS experiment on the precursor ion, with their resulting fragment ions (second generation) being analyzed by Q3. Note that at DP=40 V, secondary fragmentations already occur, however we used 60 V to increase the intensity of the fragment ions and ultimately the signal-to-noise ratio of the pseudo-MS3 spectra. During tandem experiments, ions are collisionally cooled within Q0 and Q1, located before Q2, but increasing the voltage was not meant to act on the cooling. Using either DP=40 V or 60 V results in similar pseudo-MS3 spectra. For the sake of simplicity, we refer to these results as MS/MS/MS spectra.

Chemical dynamics simulations. QM + MM chemical dynamics simulations[22] were performed to model CID of protonated disaccharides. As in our previous work,[12] we have used as projectile the argon atom. The collision system constituted by the protonated [saccharide]H^+ cation and the Ar atom was described by the following potential energy function:

$$V = V_{SaccharideH^+} + V_{Ar-Saccharide} \quad (1)$$

where $V_{SaccharideH+}$ is the intramolecular potential of the protonated saccharide cation and $V_{Ar\text{-}Saccharide}$ is the Ar/[saccharide]H^+ intermolecular potential. The PM3 semi-empirical Hamiltonian has been used for the intramolecular potential.[23] The reliability of such semi-empirical Hamiltonian to model CID processes of carbohydrates was established in previous work on galactose-6-sulfate.[13] Event if new semi-empirical methods are now available, our work on sugars, as well as more recently on peptides,[24] have shown that PM3 is able to correctly describe different systems in both positive and negative modes. Surely studying the impact of the method on the fragmentation products will be an interesting topic, which is, however, beyond the aim of the present work.

The intermolecular potential between the collision gas (Ar) and the atoms of the saccharide ion is expressed as a sum of two-body terms as follows:

$$V_{Ar-Saccharide} = \sum_i A_{Ar-i} e^{-B_{Ar-i} r_{Ar-i}} + \frac{C_{Ar-i}}{r_{Ar-i}^9} \quad (2)$$

where *i* runs over all the atoms of the [saccharide]H^+ molecular ion. We used the purely repulsive potential developed and discussed by Meroueh and Hase,[25] in which A, B and C are positive.

Note that we used Ar as collision gas in simulations while in experiments N_2 was used instead. Previous works of our group have shown that the main difference between the two gases is that the former provides a more efficient energy transfer and higher reaction probability with respect to the second.[26] Thus, to increase the reactivity and indirectly the computational efficiency we used Ar in simulations. Furthermore, we have to take into account that simulations model a single collision, while in experiments more collision can occur, thus increasing the activation energy given to the ion.

Simulations of Ar-[saccharide]H^+ collisions were done using as reference structures the minimum energy structure of each system. To obtain reliable minimum energy structures we have first performed a fast conformational search at the PM3 level, then we have selected the most stable structures and used the B3LYP/6-31+G(d,p) level of theory[27] to identify the most stable conformation. Then, harmonic vibrational frequencies were obtained at the same level to assess that the structures found corresponded to local minima. Finally, we have re-optimized these structures with PM3 to obtain a minimum which can be used as initial structure in dynamics. These initial structures are reported in the Supporting Information. Optimizations were made using Gaussian 09 suite of programs.[28]

Initial conditions in position and momenta of the [saccharide]H^+ for chemical dynamics were chosen by adding a quasi-classical 300 K Boltzmann distribution of vibrational/rotational energies about the isomer's potential energy minima.[29] Energies for the normal modes of vibration were selected from 300 K Boltzmann distribution. The resulting normal mode energies were partitioned between kinetic and potential energies by choosing a random phase of each normal mode. A 300 K rotational energy of RT/2 was added to each principal axis of rotation for the ion. Vibrational and rotational energies were transformed into Cartesian coordinates and momenta following well-known algorithms implemented in VENUS.[30] The cation was then randomly rotated

10.1002/cphc.201700202

about its Euler angles to take into account the random direction of the collision between Ar and the [saccharide]H$^+$ cation. Relative velocities were then added to the Ar/[saccharide]H$^+$ system consistently with the center-of-mass collision energy and impact parameter. Collision energy in the center-of-mass framework of 450 kcal/mol (19.51 eV) was employed in order to have enough reactive trajectories from which a reasonable sampling of different pathways was possible. The impact parameter b was randomly sampled between 0 and 5.0 Å; this latter value was chosen based on the molecular size and by energy transfer calculations showing that for b > 5.0 Å the transferred energy is less than 10% of the collision energy (and the reactivity consequently drops to zero), as shown in Figure S1 of the supporting information. The trajectories were calculated using a software package consisting of the general chemical dynamics computer program VENUS96[30] coupled to MOPAC.[31] The latter was used to calculate the potential energy and gradient for [saccharide]H$^+$ intramolecular potential. The classical equations of motion were integrated using the velocity Verlet algorithm[32] with a time step of 0.2 fs that gives energy conservation for reactive and nonreactive trajectories, as for systems we have previously investigated.[12,13,26] The trajectories were initiated at ion-projectile distance of 15 Å, large enough to guarantee no interaction between the ion and the colliding atom, and halted at a distance of 300 Å to allow substantial intramolecular motion of the sugar ion. This corresponds to a total integration time of about 5 ps. The trajectories in which the ions dissociated were also stopped. In this case, the criterion distance of 7 Å was used to guarantee no interaction between the fragments. Approximately 8000 trajectories were performed for each system, 4 to 5 % being reactive, depending on the system investigated.

MS/MS/MS fragmentations are obtained as for MS/MS, just using as initial structure the fragmentation products, which were optimized in order to have correct quasi-classical initial conditions. From simulations it is possible to obtain theoretical (time-dependent) MS/MS and MS/MS/MS spectra just counting the number of each fragment obtained at the end of the simulations. Relative intensities are then obtained just setting to 100 the most intense peak and scaling the other accordingly, as done in MS/MS and MS/MS/MS experimental spectra.

a)

b)

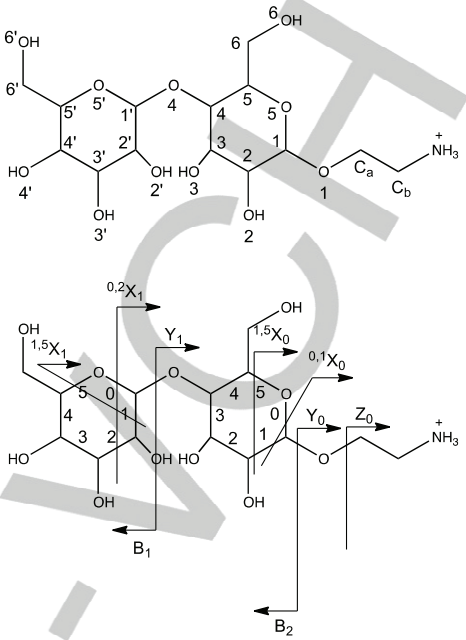

Scheme 3. a) Atom numbering, and b) bond numbering and fragmentation paths notation for β-aminoethyl-cellobiose and β-aminoethyl-maltose.

Results and Discussion

Experimental ESI-MS/MS. Fragmentation of sugars under CID conditions is a very rich phenomenon, since they can fragment through glycosidic bond or cross-ring cleavages, as well as loss of neutral molecules. Scheme 3a presents the atoms numbering, and to describe the bond that are broken, we employ the nomenclature introduced by Domon and Costello[33] (Scheme 3b). All the synthesized di-saccharides were electrosprayed and the ion corresponding to the protonated species was selected for MS/MS. The experimental ESI-MS/MS spectra exhibit many product ions even if only one basic site (the terminal amino group) is probably predominantly protonated, reflecting that different fragmentation pathways are opened. The MS/MS spectra of β-aminoethyl-disaccharides are reported in Figure 1 (the MS/MS spectra obtained for β-aminopropyl derivatives are given in Figure S2 of the supporting information). Examination of Figure 1 shows that there are no remarkable *m/z* differences between these spectra. The three isomers indeed have the same ESI/MS-MS spectra in terms of the fragment ions present. Therefore MS/MS cannot be presently easily used to distinguish the three disaccharides. Note however that the abundance of several peaks, and more particularly of *m/z* 62 and 206 ions, varies significantly according to the isomer considered, which can be of particular interest for analytical purpose.

10.1002/cphc.201700202

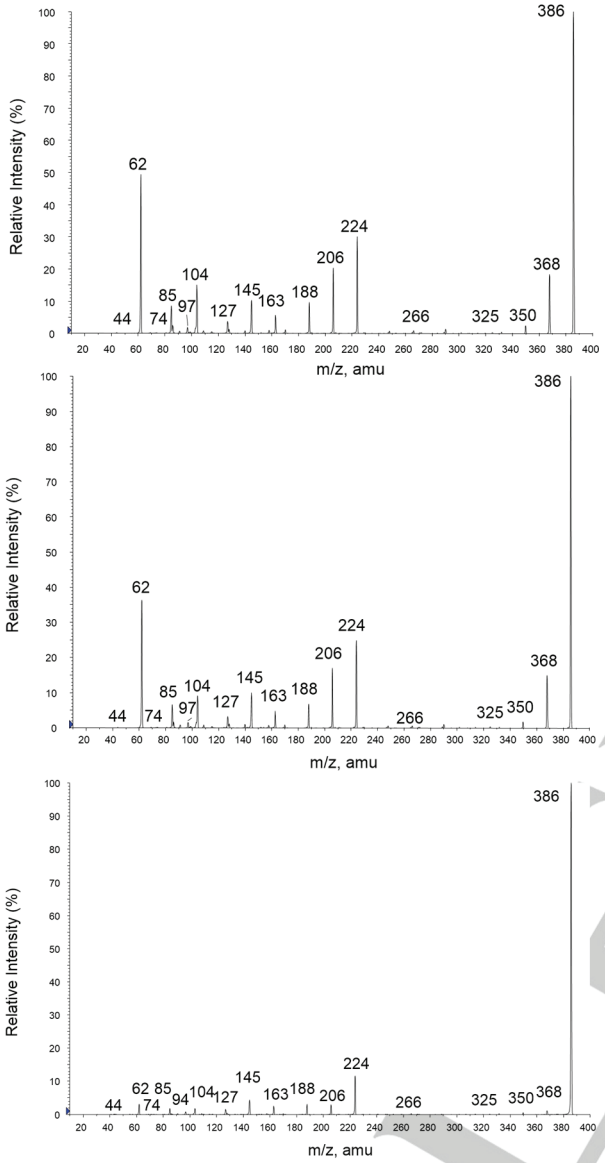

Figure 1. Experimental ESI-MS/MS of β-aminoethyl cellobiose (top), maltose (middle) and gentiobiose (bottom). Spectra were recorded with a collision energy of 25 eV in the laboratory framework.

One of the most important peak is *m/z* 368 that corresponds to H_2O loss. Another characteristic and abundant peak is *m/z* 224, likely Y_1 ion, associated with the cleavage of the glycosidic bond. We will now show how chemical dynamics simulations can be used to identify the product ions and to suggest mechanisms that may account for each fragment.

Chemical dynamics simulations of MS/MS. Using as starting structures the minimum energy structures shown in Figure S3, we have performed collisional dynamics simulations to mimic present MS/MS conditions. In Figure 2 we show the distribution of fragments obtained from CID chemical dynamics simulations of β-aminoethyl-cellobiose (a similar pattern is obtained for β-aminoethyl-maltose, see Figure S4 of the supporting information) and β-aminoethyl-gentiobiose. Note that in simulations the fragmentation patterns do not depend on the isomer considered, but intensities are generally lower for β-aminoethyl-gentiobiose, similarly to what obtained experimentally. In simulations, the peak at *m/z* 62 is too low to be compared but the peak at *m/z* 224, which has a relatively high intensity in cellobiose and maltose derivatives, is smaller in the case of β-aminoethyl-gentiobiose, reflecting what is observed during experiments.

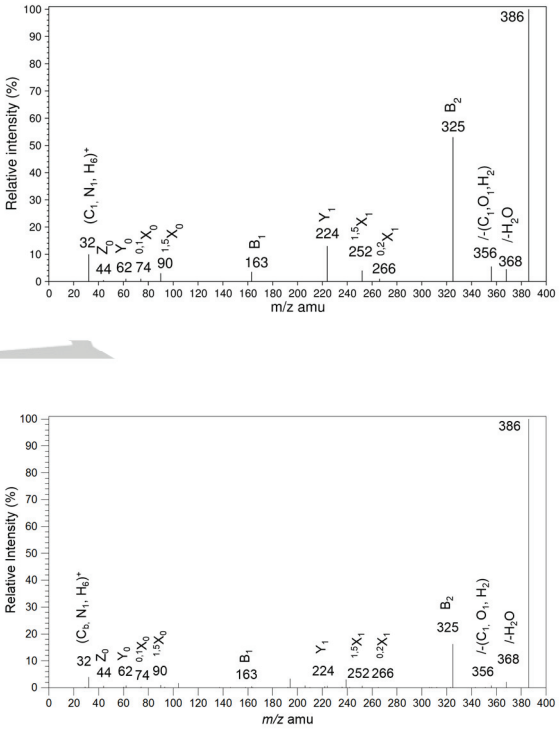

Figure 2. Fragmentation distribution of product ions obtained from CID chemical dynamics simulations of β-aminoethyl-cellobiose (upper panel) and β-aminoethyl gentiobiose (lower panel).

By inspecting the structure of the different simulation products, we can assign for each peak the corresponding structures and the bond breaking sites. They were thus reported to the theoretical fragment *m/z* distribution of Figure 2. Both glycosidic bond- (B, Y and Z ions) and cross-ring cleavages (X ions) are observed.

10.1002/cphc.201700202

Table 1. List of MS/MS and MS/MS/MS fragments for β-aminoethyl-cellobiose obtained in experiments and theory. Precursor ions are labeled as p.i.

Fragment (m/z)	MS^{2}[a]	MS^{3} (368)[b]	MS^{3} (224)[c]	MS^{2} th.[d]	MS^{3} th.[e] (368)	MS^{3} th[f] (224)
386	p.i.			p.i.		
368	✓	p.i.		✓	p.i.	
356	-	-		✓	-	
350	✓	✓		-	-	
332	-	✓		-	-	
325	✓	-		✓	-	
290	-	✓		-	-	
266	✓	-		✓	-	
252	-	-		✓	-	
248	-	✓		-	-	
224	✓	-	p.i.	✓	-	p.i.
206	✓	✓	✓	-	✓	✓
188	✓	✓	✓	-	-	-
170	-	✓	✓	-	-	-
163	✓	-	-	✓	-	-
158	-	✓	✓	-	-	-
152	-	-	✓	-	-	-
145	✓	✓	✓	-	-	-
140	-	✓	✓	-	-	-
127	✓	✓	✓	-	-	-
104	✓	✓	✓	-	-	✓
97	✓	✓	✓	-	-	-
90	-	-	-	✓	-	-
86	-	-	✓	-	-	-
85	✓	✓	✓	-	-	-
74	✓	-	✓	✓	-	-
62	✓	-	✓	✓	-	✓
44	✓	-	✓	✓	-	-
33	-	-	-	✓	-	-

[a] Experimental MS/MS; [b] Experimental MS/MS/MS from *m/z* 368 precursor ion; [c] Experimental MS/MS/MS from *m/z* 224 precursor ion; [d] Theoretical MS/MS; [e] Theoretical MS/MS/MS from *m/z* 368 precursor ion; [f] Theoretical MS/MS/MS from *m/z* 224 precursor ion.

First, comparing the theoretical fragmentation pattern with the experimental one, we can notice that most of the fragments obtained in simulations are also present in experiments, in particular the most abundant ones (while the opposite does not hold, as we will discuss later). The list of ions observed in CID chemical dynamics is reported in Table 1, where they are compared to those obtained in experiments. Since experimental and simulation conditions are not the exactly the same (and in particular simulations are in the ps time-scale, such that only fast processes can be probed), the intensities are not comparable. In fact, in collisional simulations products obtained through a fast process are overestimated, while slow pathways (generally obtained through a statistical unimolecular fragmentation) are less sampled, and they can be not seen at all. For a deeper discussion on such differences and on the problem of reproducing intensities, more details are given elsewhere.[12b,34] In general "shattering" mechanisms are better sampled, and to reproduce correctly the slow processes, information on transition states are needed to then study the kinetics via, for example, RRKM analysis or via post-TS dynamics, as recently discussed for a smaller system.[35] We now discuss some relevant peaks for which discrepancies in intensities can be rationalized due to lack of simulation time. Of course, the intrinsic limitation in using a semi-empirical Hamiltonian should always be considered as a source of error. Finally, we should remark that intensities also depend on other instrumental specificities (ionization process, mass filters and/or detector, for example) and it is not unusual that the same ion exhibits different intensities in MS/MS spectra according to the instrument used.

In the present case, we should notice that the B_2 ion (*m/z* 325) is intense in simulations, while it is small in the experimental spectrum. On the other hand, the *m/z* 224 ion, Y_1, shows similar intensities in experiments and simulations. The other ions, namely *m/z* 368 (H_2O loss), *m/z* 266 ($^{0,2}X_1$), *m/z* 163 (B_1), *m/z* 74 ($^{0,1}X_0$), *m/z* 62 (Y_0) and *m/z* 44 (Z_0), are present in both experiments and simulations, and only *m/z* 356, *m/z* 252 ($^{1,5}X_1$), *m/z* 90 ($^{1,5}X_0$) and *m/z* 32 are only present in simulations.

Globally, the reasonable agreement between experiments and simulations in identifying the principal fragmentation pattern (in particular concerning the heaviest ions) suggests that the trajectories obtained can be useful to clarify the associated mechanisms, and in particular the primary fragmentations. The absence of lighter ions in simulations will be discussed together with MS/MS/MS experiments and simulations.

In the following, we describe the mechanisms directly observed during chemical dynamics simulations of the collision between the precursor ion, *m/z* 386, and the projectile. More particularly, we provide details about the MS/MS spectrum of protonated β-aminoethyl-cellobiose (for the other sugars the mechanisms are the same).

10.1002/cphc.201700202

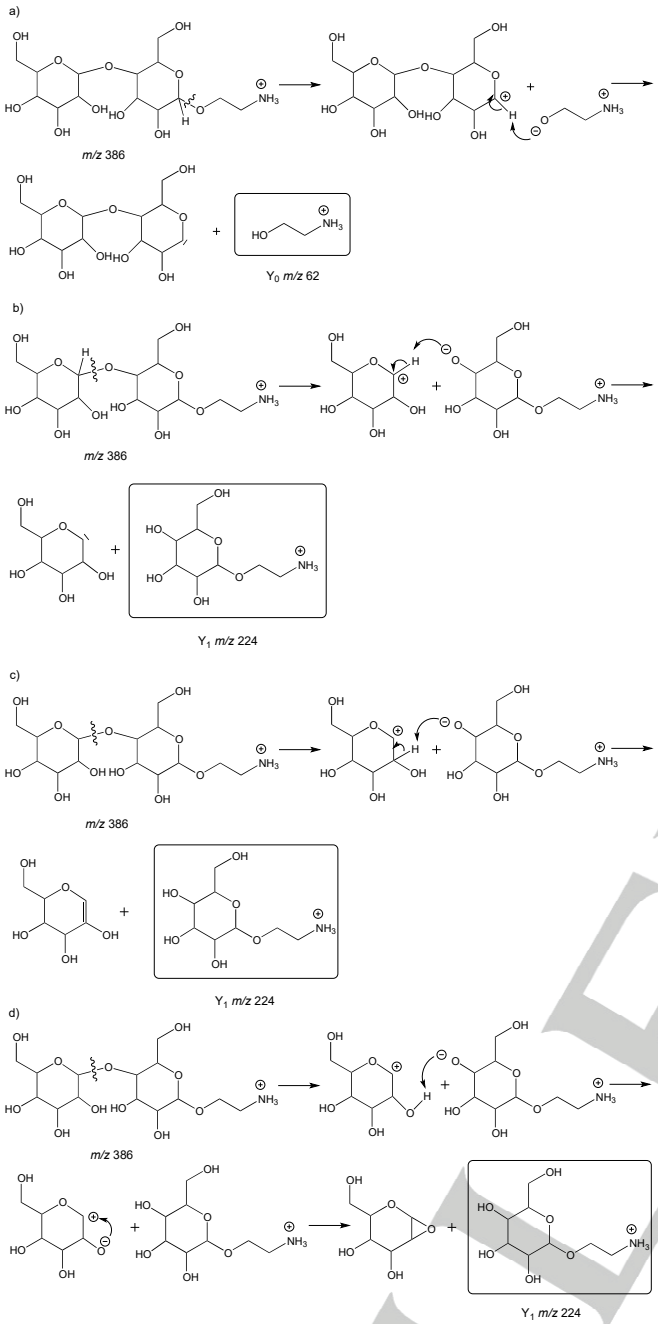

Scheme 4. Formation mechanisms of Y_0 (*m/z* 62, panel a) and Y_1 (*m/z* 224, panels b, c and d) ions from CID simulations. The ratio of the three possible pathways leading to Y_1 as obtained by CID simulations is as follows: b) 75%, c) 20% and d) 5%.

The mechanisms observed during simulations are sometimes very simple: the projectile hits the molecule and quickly after one bond is broken and the product ion is obtained. This is the case for the formation of Y_0 (*m/z* 62) and Y_1 (*m/z* 224) ions: after the C-O bond scission (C_1-O_1 and C_1-O_4, respectively) a proton is transferred forming the leaving ions, as shown in Scheme 4. Formation of either an unsaturated ring (Scheme 4c) or an epoxy form (Scheme 4d) within the leaving neutral fragment is observed during simulations, in agreement with mechanisms proposed in the literature for glycosidic bond cleavages. [9a,10a,36] Simulations also lead to the formation of a carbene neutral (Scheme 4b). We tried to perform isotope labelling (H/D exchange) experiments but unfortunately, we failed in exchanging all the exchangeable hydrogen atoms under our triple-quadrupole conditions. On the other hand, we did the experiment in a quadrupole ion trap (Figure S5). Experimentally, one can see that the Y_1 ion (*m/z* 224) is shifted both to *m/z* 230 (minor) and 231 (prominent). These *m/z* ratios are consistent with the mechanisms depicted in schemes 4b-c (6 exchangeable protons) and scheme 4d (7 exchangeable protons), respectively. We can also note that the Y_1 ion (*m/z* 224) is less intense for β-aminoethyl-gentiobiose (Figure 1c). The mechanism suggests the origin of this difference, namely the type of glycosidic bond (1,6 vs 1,4) and formation of Y_1 is due to such bond cleavage.

As just mentioned, based on our calculations the Y_1 ion could be generated according to three mechanisms, leading to the same ion but different neutral fragments. We successfully minimized (i.e obtaining real frequencies) these three neutrals at both PM3, B3LYP/6-31+G(d,p) and MP2/6-31+G(d,p) levels of theory. The alkenic form (Scheme 4c) is the most stable one, followed by the epoxy one (Scheme 4d, which is 20, 11 and 8 kcal/mol higher in energy at PM3, B3LYP and MP2 level, respectively), the carbene (Scheme 4b) being the less stable one (by 36, 45 and 50 kcal/mol at PM3, B3LYP and MP2 level, respectively). Note that the abundance obtained does not reflect the energy ordering. Probably the carbene abundance is overestimated due to the energy underestimation at PM3 level with respect to B3LYP and MP2, and, conversely, the epoxy structure is probably underestimated in simulations. However, these results clearly show how dynamical effects can be responsible of the formation of high-energy structures in mass spectra.[37]

In a recent paper by Bythell et al. the mechanisms implying a proton mobilization for the glycosidic bond cleavage was suggested from calculations locating minima and TSs.[9-b] In the present simulations, we could not observe any proton transfer to the oxygen atom of the glycosidic bond. As already mentioned, direct collisional simulations provide the amount of energy in one shock, and trajectories are not obliged to follow the minimum energy path (i.e. the path connecting minima and TSs). However, a mobile proton model mechanism is certainly a possible alternative to generate the fragment ions. We have shown recently for peptide fragmentation, that internal energy activation simulations[24] are more prone to provide proton transfers. Surely, they can be used to consider this possibility to study sugar fragmentation.

In the case of cross-ring cleavages (X ions), dissociation mechanisms observed during simulations are also simple: two bonds are broken and the products are directly obtained. In the case of $^{0,2}X_1$ ions (*m/z* 266) this can happen either by cleaving sequentially the $C_{2'}$-$C_{3'}$ and $C_{4'}$-$C_{5'}$ bonds (Scheme 5a) or by first breaking the $C_{4'}$-$C_{5'}$ bond and then, due to a concerted bond rearrangement, the $C_{2'}$-$C_{3'}$ bond (Scheme 5b). In both cases the same products (both ions and neutrals) are obtained.

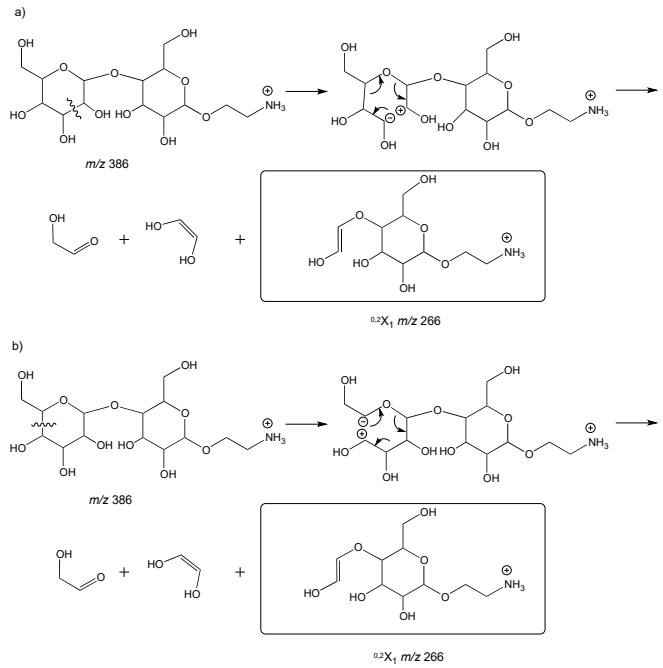

Scheme 5. Formation mechanisms of $^{0,2}X_1$ ion (*m/z* 266) from CID simulations. The two pathways are obtained in simulations with equal probability.

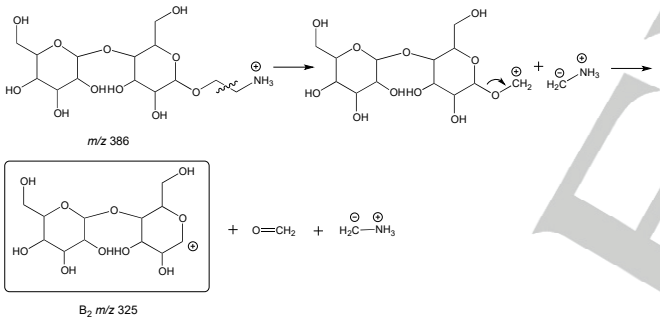

Scheme 6. Formation mechanisms of B_2 ion (*m/z* 325) from CID simulations.

The simulated mechanism leading to the B_2 ion (*m/z* 325) is a bit more complex: first the C_a-C_b bond is broken followed by the C_1-O_1 bond, with the charge now located on the B_2 side, as shown in Scheme 6. Note that this peak is very abundant in simulations while it is not in experiments. This can be due to (at least) two effects: (i) the mechanism observed in simulations is fast and not statistical (as it often happens for bond cleavages involving external groups[12d,12f]) and thus chemical dynamics overestimate its occurrence here. Another possible explanation (ii) is that the B_2 ion formed can further fragment and this process occurs in time scales longer than what available in simulations, thus increasing its relative abundance in simulations. Unfortunately, since experimentally the intensity of *m/z* 325 is very weak, it was not possible to record its fragmentation spectrum. One should also note that while *m/z* 325 is overestimated in simulations, the opposite occurs for *m/z* 62. These discrepancies illustrate the difference of conditions between experiments and simulations. These two ions are associated with the cleavage of the same bond (C_1-O_1). Experimentally, the time scale being much longer, alternate mechanisms can occur, and notably the transient formation of a proton bound dimer after this particular bond scission. Within this proton bond dimer a proton transfer between the two fragments may occur, leading to an intense *m/z* 62 ion instead of *m/z* 325. Unfortunately, such proton bound dimers were never observed in simulations.

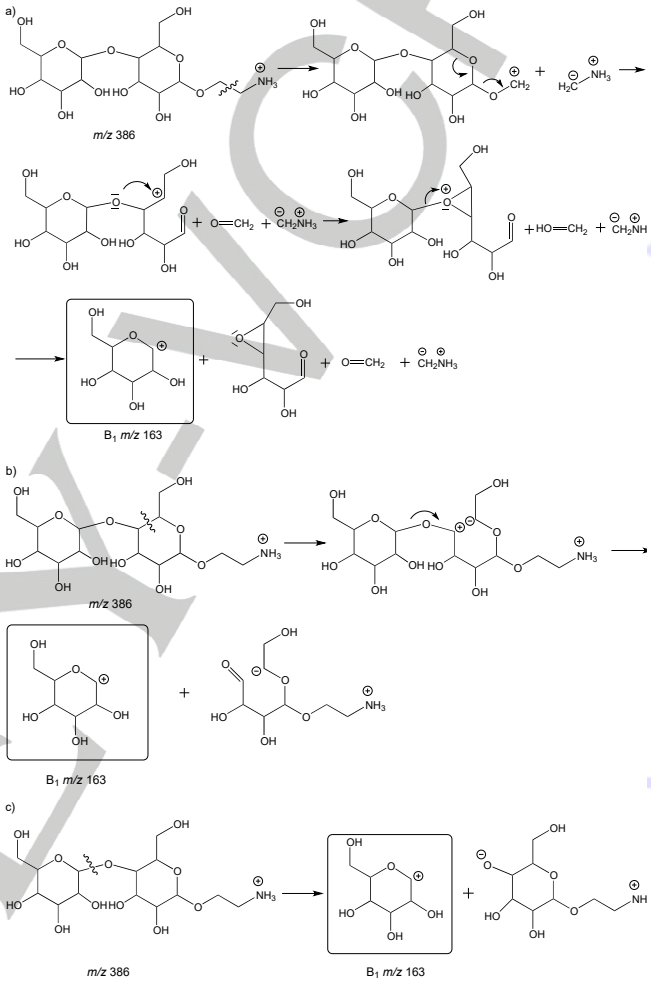

Scheme 7. Formation mechanisms of B_1 ions (*m/z* 163) from CID simulations. The ratio of the different pathways is as follows: a) 16.7%, b) 16.7%, c) 33.2%. The other mechanisms forming B_1 are reported in Scheme S1 of the SI and the ratio is: S1-a) 16.7%, S1-b) 16.7%.

Based on our chemical dynamics simulations, three types of fragmentations were observed for the formation of the B_1 ion: (1) the C_a-C_b bond is broken just after collision (charge direct mechanism) followed by cleavage of C_1-O_1 bond. At this point we have obtained an unstable B_2 ion which further fragments at the C_1-O_4 position, leading to the *m/z* 163 ion. This mechanism is shown in Scheme 7a. (2) The second possibility is that a bond of the reducing ring is first broken, then promoting the cleavage of the C_1-O_4 bond. An example is given in Scheme 7b and others in Scheme S1 of the supporting information. (3) Finally, the B_1 fragment ion can be obtained by direct cleavage of the C_1-O_4 bond after collision (see Scheme 7c). Note that we only obtained

few trajectories leading to B_1 fragment and therefore the ratios here estimated for the formation of B_1 do not necessarily reflect the actual branching ratios.

Two mechanisms are generally proposed in the literature for water loss, which differ by the origin of the accompanying hydrogen atom eliminated. The first one implies the elimination of a hydrogen atom coming from an adjacent hydroxyl group, leading to an epoxy form. This mechanism has been proposed in many studies and is supported by isotope labeling experiments.[38] The second mechanism, implying the elimination of a hydrogen atom attached to and adjacent carbon atom and leading to the formation of a double bond,[36d,39] corresponds to what is observed in the present simulations. The first step presently observed for the formation of *m/z* 368 is indeed the cleavage of one various C-O(H) bond. Then, when the OH^- is expelled and takes a proton from one nearby C-H, producing H_2O and an unsaturated moiety (Scheme 8). Note that in some cases we observed that the leaving OH^- group takes a proton from the same carbon atom to which it was bound, leading to a carbene structure (see Scheme S2 of the Supporting Information). PM3 and B3LYP/6-31G(d,p) calculations done on two final products associated with loss of OH from C_2, and leading either to alkene (Scheme 8b) or carbene (Scheme S2a), show that the alkene is more stable by 67 and 72 kcal/mol at PM3 and B3LYP level, respectively, but the carbene structure, even if higher in energy, is a local minimum (i.e. real frequencies). Finally, though epoxyde formation was not observed for water loss during our simulations, it cannot be discarded. H/D exchange experiments (Figure S5) indeed show that both types of hydrogens (C-H or O-H) can be eliminated during sequential losses of water.

One example corresponding to the H_2O loss is shown in Figure 3 (panel a). In this case the bonds are broken and formed at the same time as Ar hits the molecule, thus overestimating the contribution of C-H hydrogen atoms, which are spatially close to the OH^- leaving group.

A typical example of a complex reaction dynamics is reported in Figure 3-b, here for the formation of *m/z* 163 (B_1 ion): in this case the bond scission and formation occur at about 300 fs after that Ar hits the molecule.

We should also notice that derivatization of the anomeric hydroxyl group prevents the typical dehydration process involving the anomeric hydroxyl associated with the bond scission of the C_1-O_1 bond, weakened by anomeric effect. This process presently formally corresponds to the formation of the *m/z* 62 ion. Alternative routes for dehydration are therefore opened, involving other hydroxyl groups. Such alternative routes have been reported in different studies, either about deprotonated methyl-glycosides,[40] protonated lactose[9-b] or dealing with the interaction of methyl glycosides with metal ions.[38-a,39-b,41]

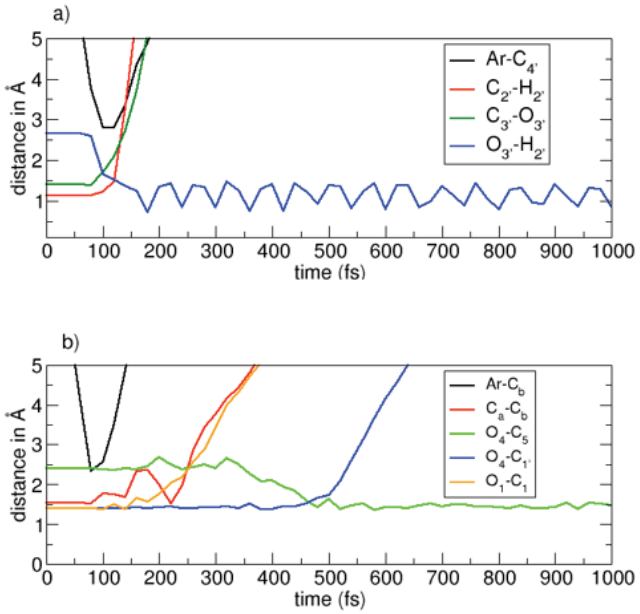

Figure 3. Evolution in time of some distances relevant for the formation of *m/z* 368 (panel a) and 163 (panel b).

Experimental MS/MS/MS. In order to gain more insights about the possible origin of low mass peaks observed experimentally in MS/MS spectra but not during the corresponding simulations, we studied the fragmentation of two product ions whose abundance was sufficient enough to record their fragmentation spectrum: *m/z* 368 and *m/z* 224. MS/MS/MS spectra of β-aminoethyl cellobiose product ions are reported in Figure 4, and those recorded for β-aminoethyl-maltose are given in Figure S6. From these MS/MS/MS spectra, we notice that most of the peaks present in the precursor ion MS/MS spectrum, are also present in MS/MS/MS spectra, except *m/z* 325, 266, 224 and 163. These latter fragments are thus only obtained from the precursor ion directly. Observation of peaks in both MS/MS and MS/MS/MS suggests that they are obtained from a secondary fragmentation of a first generation fragment ion. But this does not preclude the eventuality that they can also be produced by a primary fragmentation, as shown by Klassen's group using resonance ejection experiments.[9-a] Finally, some peaks present in MS/MS/MS spectra are not present in the precursor ion spectra: *m/z* 290, 248, 170, 158, 152, 140 and 86. Note that the same features are observed for β-aminoethyl-maltose. Hereafter, we will again only discuss mechanisms for β-aminoethyl-cellobiose.

10.1002/cphc.201700202

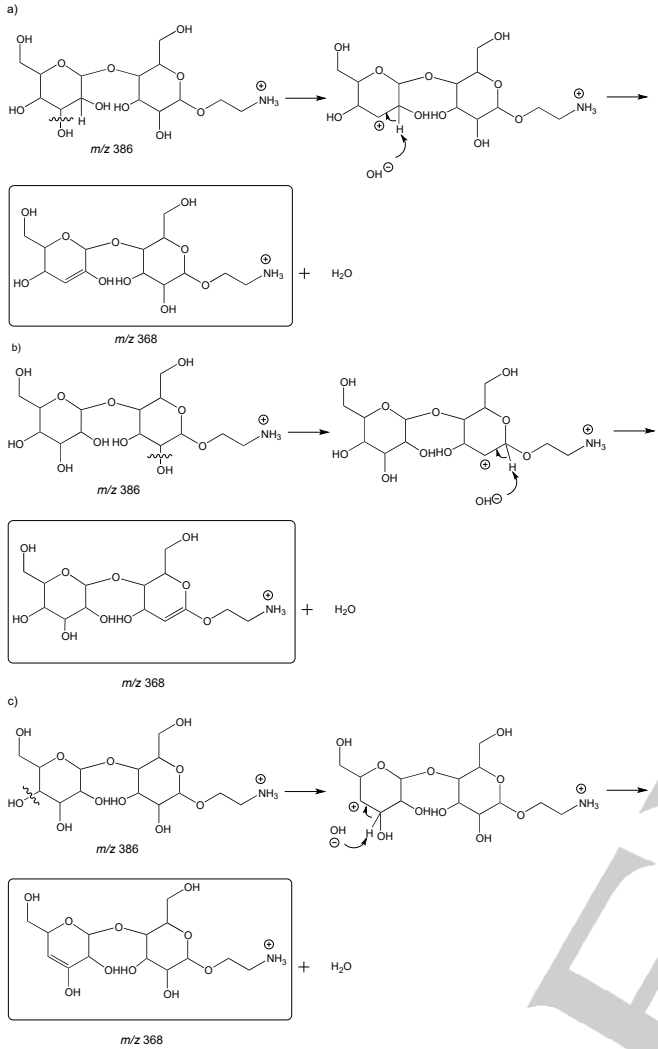

Scheme 8. Formation mechanisms of *m/z* 368 as obtained from CID simulations. The ratio of the different pathways obtained from simulations is as follows: a) 27.3%, b) 18.2%, c) 9.0%. The other mechanisms are reported in Scheme S2 of the SI and the ratio is: S2-a) 27.3%, S2-b) 18.2%.

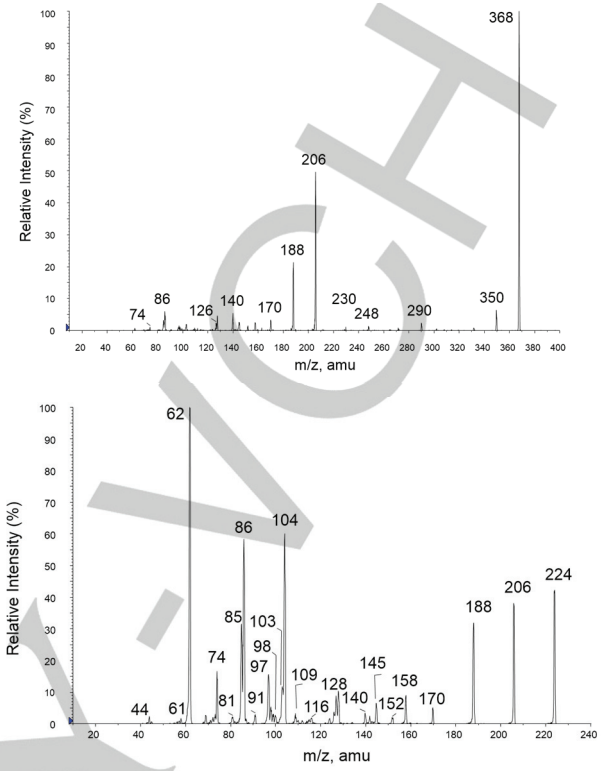

Figure 4. Experimental MS/MS/MS of β-aminoethyl cellobiose from two different precursor ions: *m/z* 368, H_2O neutral loss (upper panel), and *m/z* 224, Y_1, ion (lower panel). Spectra were recorded with a collision energy of 25 eV in the laboratory framework.

Most of the peaks present in MS/MS/MS spectra are not obtained in theoretical CID simulations of the precursor ion *m/z* 386. This suggests, together with the analysis of MS/MS and MS/MS/MS experiments, that these ions can be produced by the successive fragmentation of a first-generation fragment. However, the low mass peaks (*m/z* 74, 62 and 44) are obtained in simulations, MS/MS experiments and MS/MS/MS experiments from *m/z* 224 ion.

MS/MS/MS Simulations. In order to understand how peaks present in the MS/MS spectrum can be obtained from secondary fragmentations, we have performed MS/MS/MS simulations of the same two ions studied experimentally, namely *m/z* 368 and *m/z* 224. Results, in terms of fragments observed, are summarized in Table 1, from which simulations can be compared with experiments. The first difference is that, while the experimental MS/MS/MS spectra present a significant number of peaks, simulations only show few fragments: only one product ion, *m/z* 206, for *m/z* 368, and three product ions, *m/z* 206, 104 and 62 when the precursor ion is *m/z* 224.
The mechanism observed during simulations for the formation of *m/z* 206 from *m/z* 368 is reported in Scheme 9. We can see that

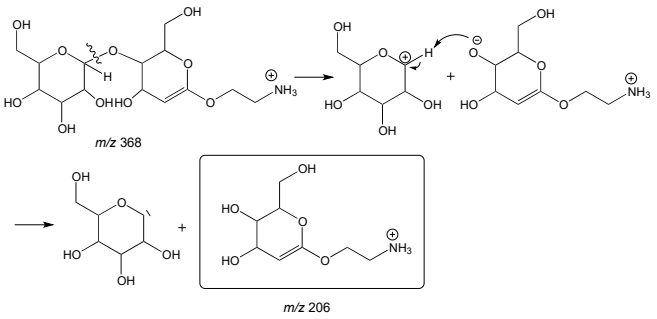

Scheme 9. Formation mechanisms of ion *m/z* 206 using as precursor ion *m/z* 368 as obtained from CID simulations.

the collision induces the cleavage of C_1-O_4 bond followed by a proton transfer on the leaving $–O^-$ group and ultimately formation of *m/z* 206. This mechanism is similar to one of the mechanism accounting for the loss of 162 Da from *m/z* 386 (scheme 4b). H/D exchange experiments (Figure S5) show that this fragment ion was shifted to *m/z* 211 and therefore incorporated 5 exchangeable protons. This result is consistent with the "scheme 8b+scheme 9" reaction sequence resulting in a structure with 5 exchangeable protons. Another important fragment observed in experiments and not in simulations is *m/z* 188, which may formally correspond to water loss from *m/z* 206. This means that *m/z* 206 may further react, this occurring at a time-scale that cannot be sampled by dynamics. Experimentally, the *m/z* 188 ion is shifted to *m/z* 191/192 when performing H/D exchanges (Figure S5), thus indicating both loss of both D_2O and HOD from *m/z* 211. Again, both types of hydrogens (C-H or O-H), are eliminated together with the hydroxyl group. It should be noted that it is not easy to give a quantitative value of the total energy transferred during MS/MS/MS experiments, since the first step in fact corresponds to "in source" fragmentation.

Concerning the *m/z* 224 ion, our simulations lead to three peaks: *m/z* 206, 104 and 62. Experimentally, there are two other peaks, *m/z* 188 and 86, which correspond to H_2O loss from *m/z* 206 and 104, respectively. They are not present in our simulations likely for the same reasons: they correspond to further fragmentation of a product that we cannot obtain due to limitation in time-scale.
The mechanisms deduced from our simulations for the formation of *m/z* 206, 104 and 62 are shown in Scheme 10. In Schemes 10a and 10b we report the two possible ways of forming *m/z* 206 according to H_2O loss: the OH^- leaving group takes an H either from the NH_3^+ tail (Scheme 10a) or from the CH group to which is attached (Scheme 10b). Note that the *m/z* 206 ion formed from *m/z* 224 has a different structure with respect to the one formed from *m/z* 368.
Formation of *m/z* 104 (see Scheme 10c) starts by the C_2-C_3 bond cleavage, followed by C_4-C_5 and C_1-O_5 bond breaking leading to three fragments. Finally, the first step leading to *m/z* 62 is the C_1-O_1 bond cleavage, followed by a proton transfer from C_1 to O_1, as shown in Scheme 10d.

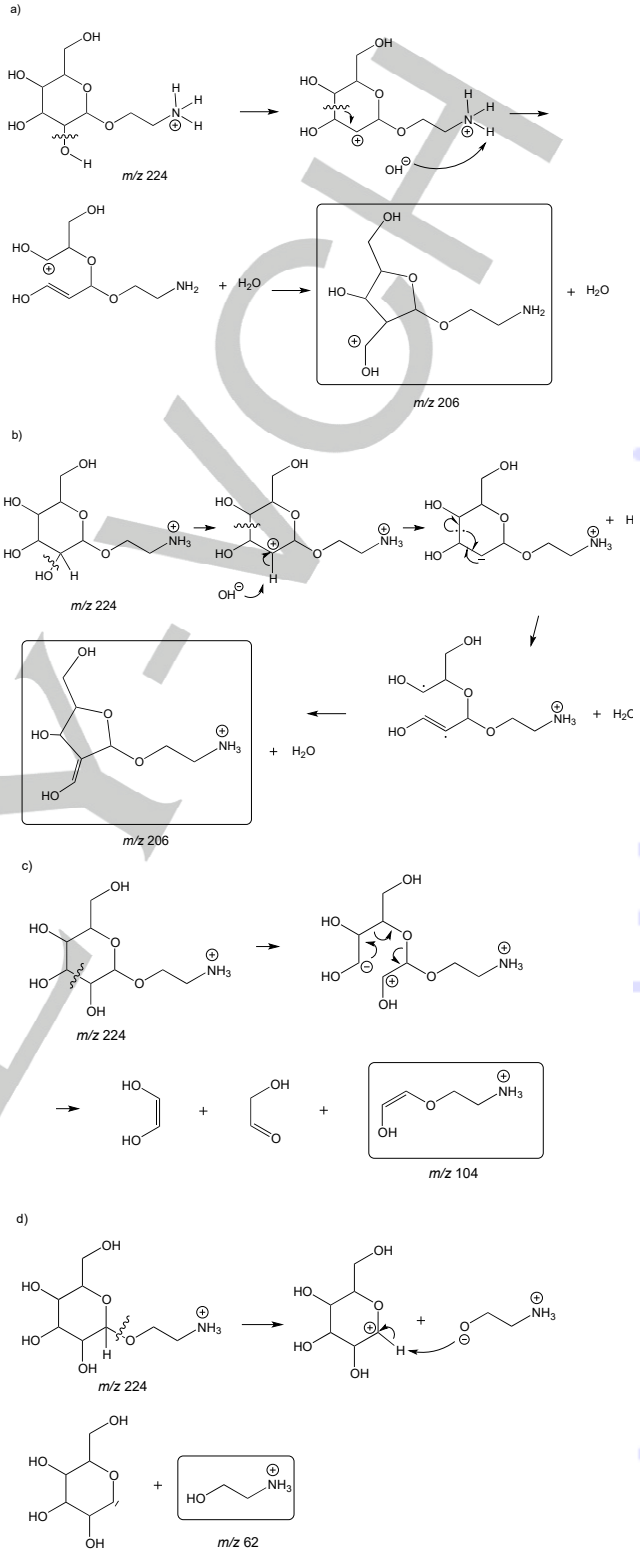

Scheme 10. Fragmentations observed using *m/z* 224 as precursor ion in CID simulations.

Conclusions

In this work, we have studied the collision-induced fragmentation of a series of disaccharides in the positive-ion mode. Sugars were modified by adding an aminoethyl or aminopropyl aglycone on the reducing end in order to unambiguously localize the additional proton and make calculations on a limited number of initial structures. Experiments show that the different disaccharides do not have a specific fragmentation pattern, which could be used to easily characterize them in a mixture. However, the differences in intensities (in particular the cellobiose/maltose derivatives *vs* the gentiobiose one) could be eventually further exploited to design a possible identification strategy, notably by coupling a liquid chromatograph to the mass spectrometer. On the other hand, the coupling between experiments and collisional chemical dynamics simulations provides a valuable tool to identify the structure of the product ions and to suggest some fragmentation mechanisms. Finally, experimental and theoretical MS/MS/MS data provide some insights about the fragments coming only from the $[M+H]^+$ ion and those which could be also obtained by subsequent fragmentation of the first generation of fragments.

Some of the simulated dissociation mechanisms are consistent with the results deduced from H/D exchange. On the other hand, these latter experiments also indicate that alternate dissociation paths not sampled by the simulations, clearly occur, probably because of the short time scale of our simulations favoring fast processes over statistical ones. The fact that we used a relatively simple semi-empirical Hamiltonian representation for the sugars' dynamics, can be an additional source of discrepancy with experiments. This is notably reflected by differences in peaks intensity and absence in simulations of some of the fragments, which are due to both small time-scale sampling and the use of approximate potential energy surface description. Another possibility is that some of the peaks present in MS/MS are generated by secondary fragmentation. This is why we performed collisional dynamics of two primary product ions providing, for the first time to our knowledge, theoretical MS/MS/MS spectra.

Acknowledgements

We thank LabEx Charm$_3$at for supporting through action ANR-11-IDEX-0003-02. R.S. and J.-Y.S. also thank ANR DynBioReact (Grant number ANR-14-CE06-0029-01) for supporting.

Keywords: Tandem mass spectrometry • Chemical dynamics • Carbohydrates • Fragmentation mechanisms

[1] a) R.A. Dwek, *Chem. Rev.* **1996**, *96*, 683-720; b) I. Bucior, M.M. Burger, *Curr. Opin. Struct. Biol.* **2004**, *14*, 631–637; c) K. Ohtsubo, J.D. Marth, *Cell* **2006**, *126*, 855–867; d) G. W. Hart, R. J. Copeland, *Cell* **2010**, *143*, 672**–**676.

[2] H.R. Morris, M.Panico, M.Barber, R.S.Bordoli, R.D.Sedgwick, A.Tyler, *Biochem. Biophys. Res. Commun.* **1981**, *101*, 623-631.

[3] M. Karas, D. Bachmann, U. Bahr, F. Hillenkamp, *Int. J. Mass Spectrom.* **1987**, *78*, 53-68.

[4] Z. Takáts, J.M. Wiseman, B.Gologan, R.G.Cook, *Science* **2004**, *5695*, 471-473.

[5] J.B. Fenn, M. Mann, C.K. Meng, S. F. Wong, C. M. Whitehouse, *Science* **1989**, *246*, 64-71.

[6] P.M. Mayer, C. Poon, *Mass Spectrom. Rev.* **2009**, *28*, 608-639.

[7] W. Hoffmann, J. Hofmann, K. Pagel, *J. Am. Soc. Mass Spectrom.* **2014**, *25*, 471-479.

[8] a) B. Paizs, S. Suhai, *Mass Spectrom. Rev.* **2004**, *24*, 508-548; b) R. Aebersold, D.R. Goodlett, *Chem. Rev.* **2001**, *101*, 269-295; c) A. G. Harrison, *Mass. Spectrom. Rev.* **2009**, *28*, 640-654; d) A.L. Patrick, N.C. Polfer, *Top. Curr. Chem.* **2015**, *364*, 153-182.

[9] a) M.A. Fentabil, R. Daneshfar, E.N. Kitova, J.S. Klassen, *J. Am. Soc. Mass Spectrom.* **2011**, 22, 2171-2178; b) B.J. Bythell, M.T. Abutokaikah, A.R. Wagoner, S. Guan, J.M. Rabus, *J. Am. Soc. Mass Spectrom.* **2017**, *28*, 688-703; c) G.E. Hofmeister, Z. Zhou, J.A. Leary, *J. Am. Chem. Soc.* **1991**, *113*, 5964-5970; d) V.N. Reinhold, B.B. Reinhold, C.E. Costello, *Anal. Chem.* **1995**, *67*, 1772-1784.

[10] a) T. Yamagaki, K. Fukui, K. Tachibana, *Anal. Chem.* **2006**, *78*, 1015-1022; b) H. Suzuki, A. Kameyama, K. Tachibana, H. Narimatsu, K. Fukui, *Anal. Chem.* **2009**, *81*, 1108-1120.

[11] a) P. de Sainte Claire, W.L. Hase, *J. Phys. Chem.* **1996**, *100*, 8190-8196; b) J. Liu, K. Song, W.L. Hase, *J. Chem. Phys.* **2003**, *119*, 3040-3050; c) E. Martinez-Nuñez, A. Fernandez-Ramos, S.A. Vazquez, J.M.C. Marques, M. Xue, W.L. Hase, *J. Chem. Phys.* **2005**, *123*, 154311; d) O. Meroueh, Y. Wang, W.L. Hase, *J. Phys. Chem. A* **2002**, *106*, 9983-9992.

[12] a) R. Spezia, J.-Y. Salpin, M.-P. Gaigeot, W.L. Hase, K. Song, *J. Phys. Chem. A* **2009**, *113*, 13853-13862; b) R. Spezia, S.B. Lee, A. Cho, K. Song, *Int. J. Mass Spectrom.* **2015**, *392*, 125-138; c) R. Spezia, J. Martens, J. Oomens, K. Song, *Int. J. Mass Spectrom.* **2015**, *388*, 40-52; d) D. Ortiz, P. Martin-Gago, A. Riera, K. Song, J.-Y. Salpin, R. Spezia, *Int. J. Mass Spectrom.* **2013**, *335*, 33-44; e) E. Rossich Molina, D. Ortiz, J.-Y. Salpin, R. Spezia, *J. Mass Spectrom.* **2015**, *50*, 1340-1351; f) R. Spezia, A. Cimas, M.-P. Gaigeot, J.-Y. Salpin, K. Song, W.L. Hase, *Phys. Chem. Chem. Phys.* **2012**, *14*, 11724-11736; g) A. Martin-Somer, M. Yañez, M.-P. Gaigeot, R. Spezia, *J. Phys. Chem. A* **2014**, *118*, 10882-10893.

[13] D. Ortiz, J.-Y. Salpin, K. Song, R. Spezia, *Int. J. Mass Spectrom.* **2014**, *358*, 25-35.

[14] a) A. Ballistreri, G. Montaudo, D. Garozzo, M. Giuffrida, G Impallomeni, S. Daolio, *Rapid Comm. Mass Spectrom.* **1989**, *3*, 302-304; b) J.W. Dallinga, W. Heerma, *Biol. Mass Spectrom.* **1991**, *20*, 215-231; c) J.A. Carroll, L. Ngoka, C.G. Beggs, C.B. Lebrilla, *Anal. Chem.* **1993**, *65*, 1582-1587; d) D. Garozzo, M. Giuffrida, G. Impallomeni, A. Ballistreri, G. Montaudo, *Anal. Chem.* **1992**, *62*, 279-286; e) J.A. Carroll, D. Willard, C.B. Lebrilla, *Anal. Chim. Acta* **1995**, *307*, 431-447; f) B. Mulroney, J.C. Traeger, B.A. Stone, *J. Mass Spectrom.* **1995**, *30*, 1277-1283; g) R.E. March, C.J. Stadey, *Rapid Comm. Mass Spectrom.* 2005, 19, 805-812.

[15] a) B. Mulroney, J.B. Peel, J.C. Traeger, *J. Mass Spectrom.* **1999**, *34*, 544-553; b) J.-Y. Salpin, J. Tortajada, *J. Mass Spectrom.* **2004**, *39*, 930-941.

[16] G. Yang, C. Zhu, L. Zhou, *J. Mol. Model.* **2016**, *22*, 104.

[17] S. Feng, C. Bagia, G. Mpourmpakis, *J. Phys. Chem. A* **2013**, *117*, 5211-5219.

[18] J. Dahmén, T. Frejd, G. Grönberg, T. Lave, G. Magnusson, G. Noori, *Carbohydr. Res.* **1983**, *116*, 303-307.

[19] a) E. F. V. Scriven, K. Turnbull, *Chem. Rev.* **1988**, *88*, 297-368; b) S. G. Alvarez, M. T. Alvarez, *Synthesis* **1997**, 413-414; c) K. Yamamoto, T. Bruun, J. Y. Kim, L. Zhang, M. Lautens, *Org. Lett.* **2016**, *18*, 2644-2647.

[20] a) G. Zemplén, E. Pascu, *Ber. Dtsch. Chem. Ges.* **1929**, *62*, 1613-1614; b) T. K. Lindhorst, in *Essentials of Carbohydrate Chemistry and Biochemistry* Eds.: Wiley-VCH Verlag GmbH & Co. KGaA, Weinheim, 2007.

[21] I.V. Chernushevich, A.V. Loboda, B.A. Thomson, *J. Mass Spectrom.* **2001**, *36*, 849-865.

[22] a) A. Rahman, W.L. Hase, K. Song, J. Wang, S.O. Meroueh in *Principles of Mass Spectrometry Applied to Biomolecules* (Eds.: J. Laskin, C. Lifshitz), Wiley, Hoboken NJ, **2006**, pp. 379-474; b) K. Bolton, W.L. Hase, G.Peslherbe in *Modern Methods for Multidimensional Dynamics Computations in Chemistry* (Ed.: D.L. Thompson), World Scientific, London, **1998**, pp. 143-189; c) L. Sun, W.L. Hase, *Rev. Comp. Chem.* **2003**, *19*, 79-146.

[23] a) J.J.P. Stewart, *J. Comp. Chem.* **1989**, *10*, 209-220; b) J.J.P. Stewart, *J. Comp. Chem.* **1989**, *10*, 221-264.

[24] R. Spezia, A. Martin-Somer, V. Macaluso, Z. Homayoon, S. Pratihar, W.L. Hase, *Faraday Discuss.* **2016**,*195*, 599-618.

[25] O. Meroueh, W.L. Hase, *J. Phys. Chem. A* **1999**, 103, 3981-3990.

[26] Y. Jeanvoine, M.-P. Gaigeot, W.L. Hase, K. Song, R. Spezia, *Int. J. Mass Spectrom.* **2011**, *308*, 289-298.

[27] a) A.D. Becke, *J. Chem. Phys.* **1993**, *98*, 1372-1377; b) C. Lee, W. Yang, R.G. Parr, *Phys. Rev. B* **1988**, *37*, 785-789.

[28] Gaussian 09, Revision D.01, M. J. Frisch, G. W. Trucks, H. B. Schlegel, G. E. □Scuseria, M. A. Robb, J. R. Cheeseman, G. Scalmani, V. Barone, B. Men- nucci, G. A. Petersson, H. Nakatsuji, M. Caricato, X. Li, H. P. Hratchian, A. F. Izmaylov, J. Bloino, G. Zheng, J. L. Sonnenberg, M. Hada, M. Ehara, K. Toyota, R. Fukuda, J. Hasegawa, M. Ishida, T. Nakajima, Y. Honda, O. Kitao, H. Nakai, T. Vreven, J. A. Montgomery, Jr., J. E. Peralta, F. Ogliaro, M. Bearpark, J. J. Heyd, E. Brothers, K. N. Kudin, V. N. Staroverov, R. Ko- bayashi, J. Normand, K. Raghavachari, A. Rendell, J. C. Burant, S. S. Iyen- gar, J. Tomasi, M. Cossi, N. Rega, N. J. Millam, M. Klene, J. E. Knox, J. B. Cross, V. Bakken, C. Adamo, J. Jaramillo, R. Gomperts, R. E. Stratmann, O. Yazyev, A. J. Austin, R. Cammi, C. Pomelli, J. W. Ochterski, R. L. Martin, K. Morokuma, V. G. Zakrzewski, G. A. Voth, P. Salvador, J. J. Dannenberg, S. Dapprich, A. D. Daniels, O. Farkas, J. B. Foresman, J. V. Ortiz, J. Cio- slowski, D. J. Fox, Gaussian, Inc., Wallingford, CT, **2009**.

[29] a) S. Chapman, D.L. Bunker, *J. Chem. Phys.* **1975**, *62*, 2890-2899; b) C.S. Sloan and W.L. Hase, *J. Chem. Phys.* **1977**, *66*, 1523-1533.

[30] a) Y.J. Cho, S.R. Vande Linde, L. Zhu, W.L. Hase, *J. Chem. Phys.* **1992**, *96*, 8275; b) X. C. Hu, W.L. Hase, T. Pirraglia, *J. Comp. Chem.* **1991**, *12*, 1014-1024; c) W.L. Hase, R.J. Duchovic, X. Hu, A. Komornicki, K. Lim, D.-H. Lu, G.H. Peslherbe, K.N. Swamy, S.R. Vande Linde, H. Wang, R.J. Wolf, *QCPE Bull.* **1996**, 16.

[31] J.J.P. Stewart, *J. Comput.-Aid. Mol. Des.* **1990**, *4*, 1-45.

[32] L. Verlet, *Phys. Rev.* **1967**, *159*, 98.

[33] B. Domon, C.E. Costello, *Glycoconjugate J.* **1988**, *5*, 397-409.

[34] E. Rossich-Molina, J.-Y. Salpin, R. Spezia, E. Martínez-Núñez, *Phys. Chem. Chem. Phys.* **2016**, *18*, 14980-14990.

[35] A. Martin-Somer, R. Spezia, M.Yanez, *Phil. Trans. A* **2017**, *375*, 20160196.

[36] a) G.E. Hofmeister, Z. Zhou, J.A. Leary, *J. Am. Chem. Soc.* **1991**, *113*, 5964-5970; b) S. Konig, J.A. Leary, *J. Am. Soc. Mass Spectrom.* **1998**, *9*, 1125-1134; c) O.M. Saad, J.A. Leary, *J. Am. Soc. Mass Spectrom.* **2004**, *15*, 1274-1286; d) S. Mendonca, R.B. Cole, J.H. Zhu, Y. Cai, A.D. French, G.P. Johnson, R.A. Laine. *J. Am. Soc. Mass Spectrom.* **2003**, *14*, 63-78; e) N. G. Karlsson, H. Karlsson, G. C. Hansson. J. Mass Spectrom. 1996, 31, 560-572; f) W. Tuting, R. Adden, P. Mischnick. *Int. J. Mass Spectrom.* **2004**, *232*, 107-115.

[37] a) R. Spezia, E. Martinez-Nunez, S. Vasquez, W.L. Hase, *Phil. Trans. A.* **2017**, *375*, 20170035 (2017); b) V. Brites, A. Cimas, R. Spezia, N. Sieffert, J.M. Lisy, M.-P. Gaigeot, *J. Chem. Theory Comput.* **2015**, *11*, 871-883, c) X. Ma, W.L. Hase, *Phil. Trans. R. Soc. A* **2017**, *375*, 20160204.

[38] a) J. M. Berjeaud, F. Couderc, J. C. Promé, *Org. Mass Spectrom.* **1993**, *28*, 455; b) K.P. Madhusudanan, *J. Mass Spectrom.* **2006**, *41*, 1096-1104; c) K.P. Madhusudanan, S. Kanojiya, B. Kumar. *J. Mass Spectrom.* **2005**, 1044-1054; d) M. R. Asam, G. L. Glish. *J. Am. Soc. Mass Spectrom* **1997**, *8*, 987-995; e) M. D. Leavell, J. A. Leary. *Int. J. Mass Spectrom.* **2001**, *204*, 185-196.

[39] a) B. Mulroney, J.B. Peel, J.C. Traeger, *J. Mass Spectrom.* **1999**, *34*, 856-871; b) J.-Y. Salpin, L. Boutreau, V. Haldys, J. Tortajada, *Eur. J. Mass Spectrom.* **2001**, *7*, 321-330; c) J. Zhang, J. S. Brodbelt, *Anal. Chem.* **2005**, *77*, 1761, 1770.

[40] J.C. Promé, H. Aurelle, D. Promé, A. Savagnac, *Org. Mass Spectrom.* **1987**, *22*, 6.

[41] J.-Y. Salpin, J. Tortajada, *J. Mass Spectrom.* **2002**, *37*, 379-388.

Entry for the Table of Contents (Please choose one layout)

Layout 1:

ARTICLE

By coupling tandem mass spectrometry experiments with chemical dynamics simulations it was possible to understand mechanisms for primary and secondary fragmentation of disaccharides.

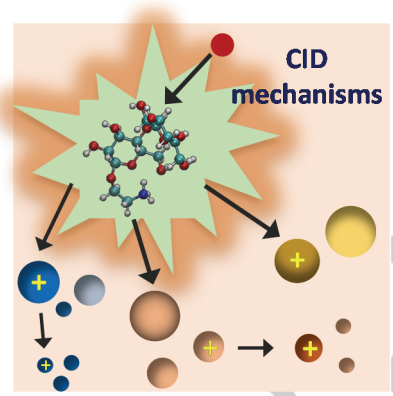

E. Rossich Molina, A. Eizaguirre, V. Haldys, D. Urban, G. Doisneau, Y. Bourdreux, J.-M. Beau, J.-Y. Salpin, R. Spezia**

Page No. – Page No.

Characterization of protonated model disaccharides from tandem mass spectrometry and chemical dynamics simulations